
Article:
Ambrogio, S., Walker, A., Narracott, A. orcid.org/0000-0002-3068-6192 et al. (3 more authors) (2019) A complex flow phantom for medical imaging : ring vortex phantom design and technical specification. Journal of Medical Engineering & Technology, 43 (3). pp. 190-201. ISSN 0309-1902

https://doi.org/10.1080/03091902.2019.1640309

A Complex Flow Phantom for Medical Imaging: Ring Vortex Phantom Design and Technical Specification

[1,2,3]Ambrogio Simone, [3]Walker Adrian, [1,2]Narracott Andrew, [1,2]Ferrari Simone, [4]Verma Prashant, [1,2]Fenner John

[1]Medical Physics, Mathematical Modelling in Medicine Group, Department of Infection, Immunity and Cardiovascular Disease, University of Sheffield, Sheffield, UK
[2]Insigneo Institute for In Silico Medicine, University of Sheffield, Sheffield, UK
[3]Leeds Test Objects Ltd., Boroughbridge, UK
[4]Medical Imaging & Medical Physics, Sheffield Teaching Hospitals NHS Foundation Trust, Sheffield, UK

Corresponding Author:
Simone Ambrogio
E-mail: simoambr@gmail.com
(Orcid 0000-0003-1571-0016)

ABSTRACT

Cardiovascular fluid dynamics exhibit complex flow patterns, such as recirculation and vortices. Quantitative analysis of these complexities supports diagnosis, leading to early prediction of pathologies. Quality Assurance of technologies that image such flows is challenging but essential, and to this end, a novel, cost-effective, portable, complex flow phantom is proposed and the design specifications are provided. The vortex ring is the flow of choice because it offers patterns comparable to physiological flows and is stable, predictable, reproducible and controllable. This design employs a piston/cylinder system for vortex ring generation, coupled to an imaging tank full of fluid, for vortex propagation. The phantom is motor-driven and by varying piston speed, piston displacement and orifice size, vortex rings with different characteristics can be produced. Two measurement methods, namely Laser-PIV and an optical/video technique, were used to test the phantom under a combination of configurations. Vortex rings with a range of travelling velocities (approximately 1-80cm/s) and different output-orifice diameters (10-25mm) were produced with reproducibility typically better than +/-10%. Although ultrasound compatibility has been demonstrated, longer-term ambitions include adapting the design to support comparative studies with different modalities, such as MRA and X-ray-CTA.

Keywords: Medical Imaging Phantom, Doppler Ultrasound Quality Assurance, Vortex Ring, Complex Flow Phantom, Laser PIV

1. Introduction

The fluid dynamics of the cardiovascular system are associated with many complexities and this has provoked interest from scientists for decades. Recirculation, turbulence, jets and vortices are observed both in healthy and pathophysiological conditions [1,2]. Quantitative analysis of the distribution of blood velocity patterns can support diagnosis of the cardiovascular system, leading to early prediction of pathologies, improvements of surgical outcomes and evaluation of potential therapies [2,3]. Magnetic Resonance angiography and Doppler Ultrasound are examples of technologies that offer valuable flow-based assessment of the cardiovascular system. 4D Flow MRI is a powerful technique that provides a time-resolved 3D velocity field. Velocity is encoded along all three spatial dimensions in the vessel of interest (4D = 3D + time). Unfortunately, this technique is not clinically routine because the acquisition time exceeds that demanded by the clinical workflow [4]. Doppler Ultrasound is portable, non-invasive, cost effective, does not involve ionizing radiation and provides qualitative and quantitative real-time information about volumes (i.e stroke volume, ejection fraction), inferred pressures (across heart valves) and flows (i.e. cardiac output) [5,6]. For these reasons, Ultrasound is currently the first choice as a diagnostic modality for the assessment of several cardiovascular pathologies [7]. Recent developments include 2D and 3D real-time angle independent Ultrasound Doppler imaging techniques, based on Vector Flow Imaging (VFI), and post-processing algorithms for particle velocimetry tracking and volume quantification [6,7,8,9,10,11,12,13]. A specific Ultrasound VFI technique - Transverse Oscillation (TO) - has been FDA approved (2013) and is clinically available on commercial scanners (eg. BK Ultrasound, Nova Scotia, Canada, and Carestream Health, Ontario, Canada) for real-time analysis of complex flows in valves, bifurcations and heart chambers [6,14]. A colour Doppler based VFI technique is also commercially available on clinical scanners manufactured by Hitachi (Hitachi Ltd., Tokyo, Japan), GE Healthcare (GE Healthcare, Illinois, USA) and Mindray (Mindray Medical International Limited, Shenzen, China). Blood speckle imaging is available on the GE Healthcare Vivid E95™ (GE Healthcare, Illinois, USA). In this domain, improved technologies for calibration of such medical imaging techniques are essential. Complex flows are needed as a standard reference for the validation of innovative flow estimation algorithms.

Recent audits concerning Ultrasound Quality Control protocols indicate that the current flow/velocity test objects available on the market are rather limited, expensive, and often fail to reproduce physiological conditions and physiological waveforms [15,16,17,18]. Manufacturers are not clear about tolerances and accuracy specifications [18] and the lack of well-defined protocols makes the Quality Control of scanners that measure flow and velocity challenging [15,16]. For example, experimental mean velocity measurements using a commercial string phantom (as recommended in IPEM Report 102, Institute of Physics and Engineering in Medicine, 2010) for linear, curvilinear and phased array probes reported errors exceeding 20%, 50% and 40%, respectively [17]. These values are considerably higher than the recommended maximum error value of +/- 5%, as declared by BS EN 61685:2002-IEC 61685:2001, a current International standard (stability date: 2020) for the development of a flow Doppler test object [19].

It is this context that is the motivation for the development of a novel phantom, designed to produce complex flows that are stable, predictable, controllable and reproducible. The particular flow chosen as the basis for the design is the vortex ring. This paper describes the salient features of a prototype ring vortex phantom providing necessary details for construction in a form suited to calibration of Ultrasound flow imaging systems. With its uniquely controllable characteristics, the ring vortex is a suitable flow reference for a flow test object.

2. Materials and Methods

The complex flow phantom design described here uses a piston to propel a slug of fluid along a cylindrical channel, through an orifice port that connects to an open tank of fluid (containing water, Blood-Mimicking Fluid etc.) where propagation of the ring may be observed and imaged. A vortex ring naturally forms when a column of fluid is pushed through an orifice into a neighbouring expansive fluid environment. The fluid propelled through the orifice "rolls up" the orifice face, forming a toroidal core of vorticity that may ultimately detach (at high enough Reynolds number) and propagates along the axisymmetric axis of the ring. The whole process is managed by computer control of piston displacement that delivers the fluid slug with a precisely specified velocity/displacement profile. Each component of the phantom is presented below followed by description of the functioning unit as a whole.

2.1 Imaging Tank

The imaging tank (Figure 1) is the principal component of the phantom since it is the environment in which the ring vortex propagates; it is the volume used to image the generated flow. The tank is manufactured from clear poly(methyl methacrylate) (PMMA) which rests on four small screw feet. These are adjustable to allow levelling of the system via two spirit levels placed on opposite walls of the tank box. The tank has internal dimensions of 15 cm (W) x 35 cm (L) x 16.5 cm (H) (Figure 1), chosen to be sufficiently large that the walls do not influence ring vortex propagation.

Several reference markers and a ruler are laser-cut into the surfaces of the tank walls to support

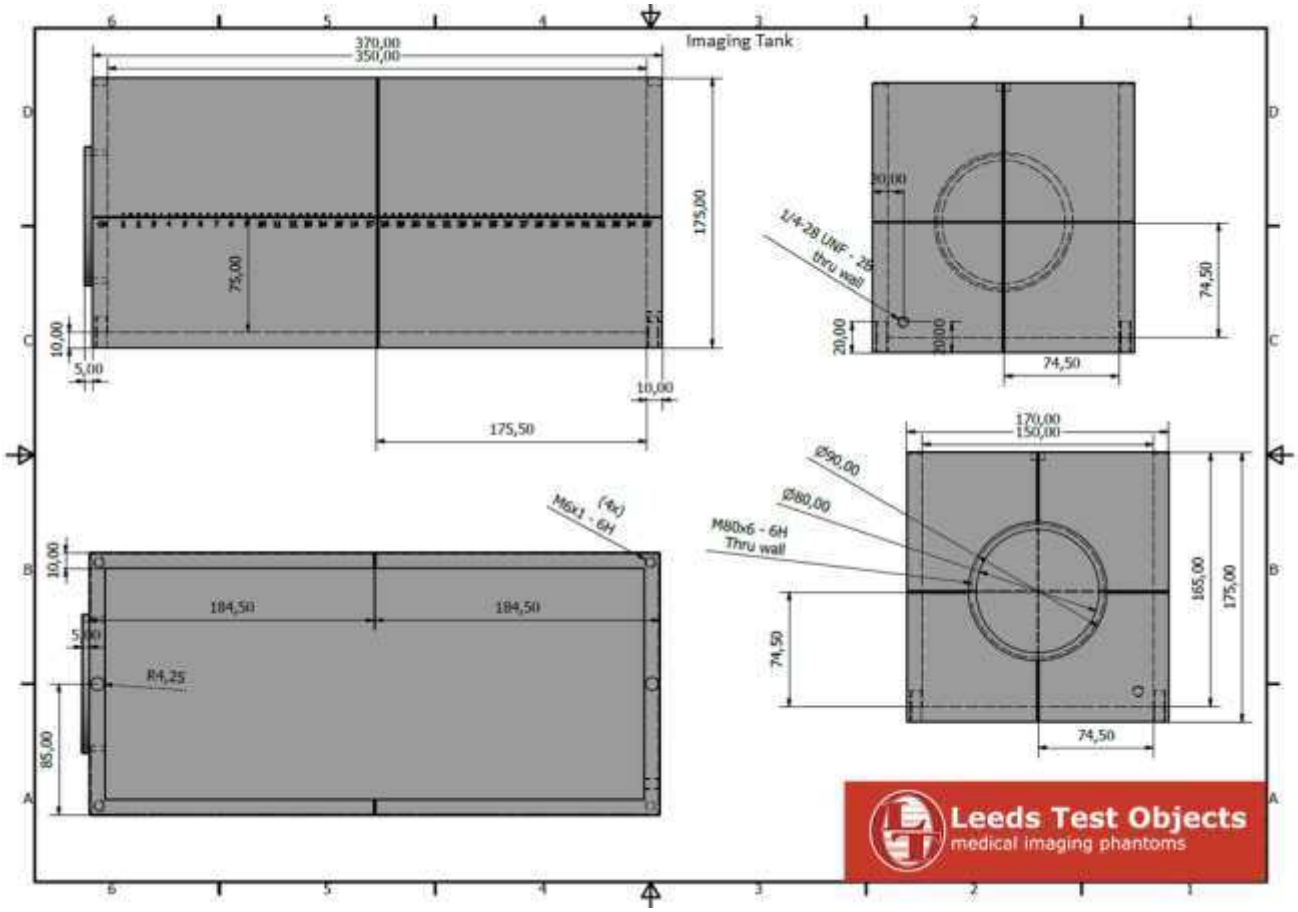

Figure 1. *CAD drawing of the ring vortex tank.*

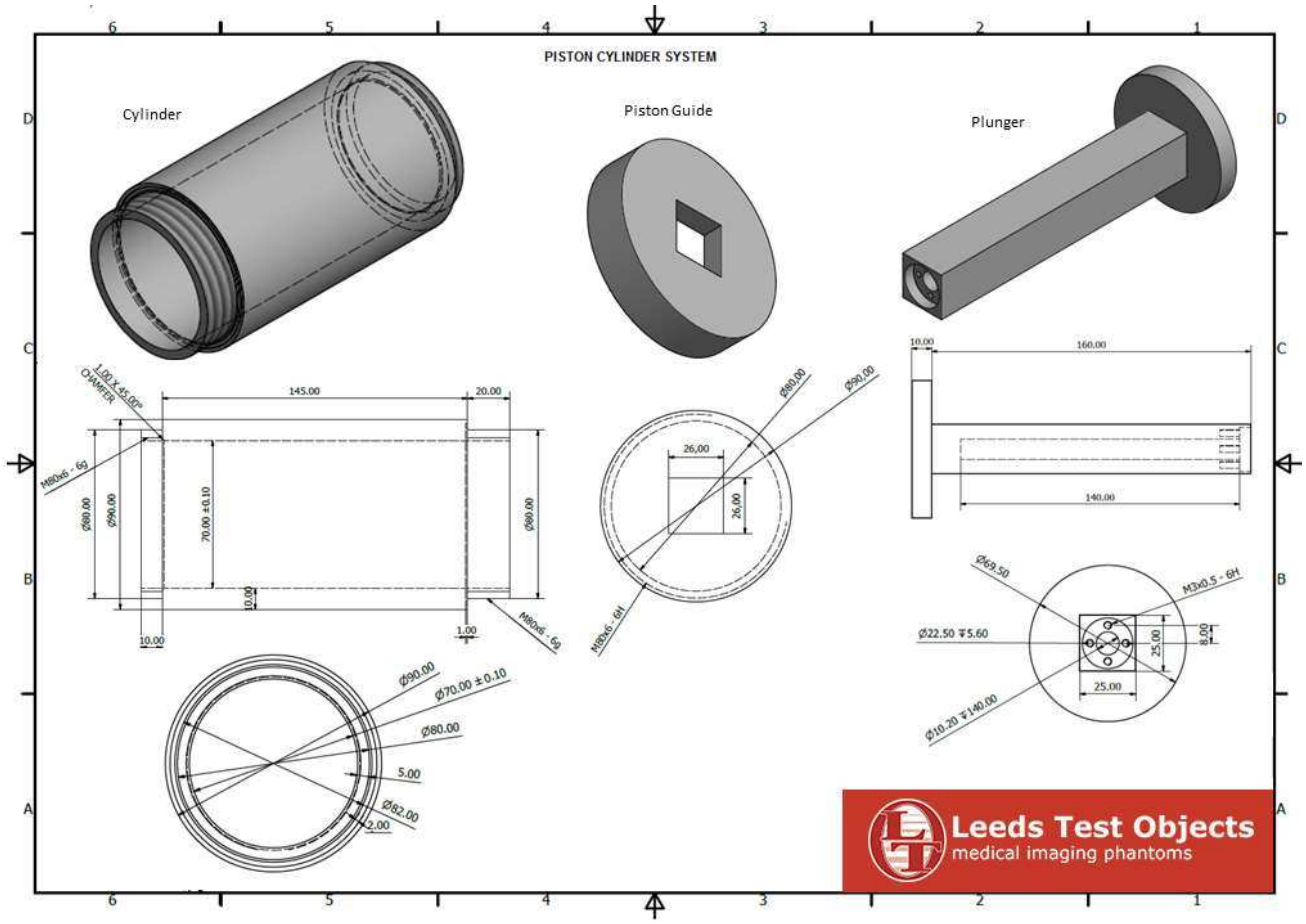

Figure 2. *CAD drawing of the piston cylinder system.*

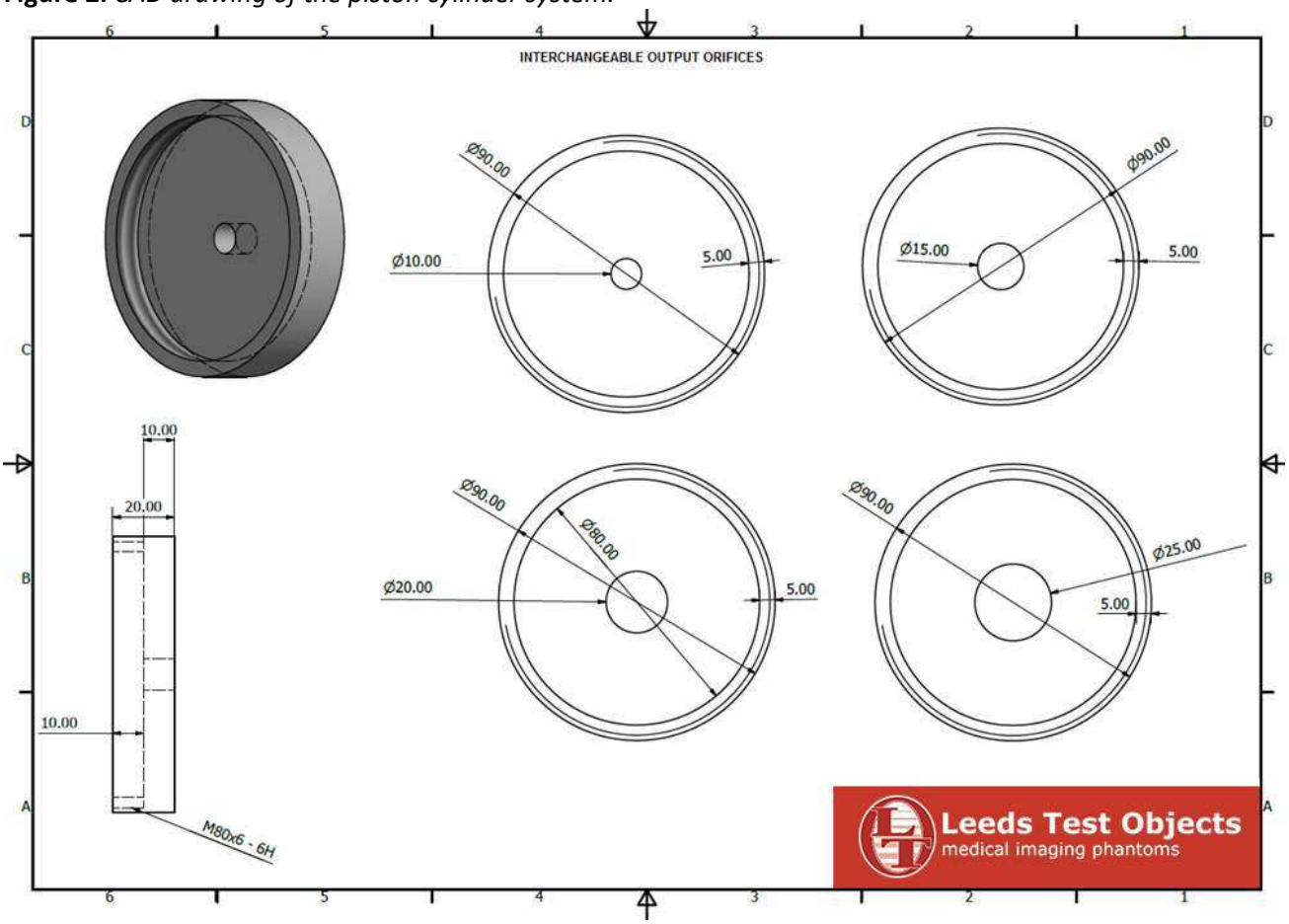

Figure 3. *CAD drawing of the attachable/detachable orifices.*

positioning and measurement. A drain is incorporated into the base of the unit to allow emptying. The top of the tank is open, offering easy access for Ultrasound imaging probes.

2.2 Piston Cylinder System

The generation of vortex rings relies on three components: a cylindrical channel, a plunger and an orifice that connects the channel to the imaging tank. The cylindrical channel used here is of internal diameter 70+/-0.10 mm, reamed from a solid cylinder manufactured from PMMA (Figure 2). The extremities of the chamber are threaded. One end of the chamber includes a screw thread for leak-proof coupling with the orifice and the imaging tank. At the other end is screwed a threaded cap, with a square hole at its centre and this acts as a piston guide (Figure 2). The plunger is made from white PMMA and its stem is of square cross-section. The plunger stem slides through the piston guide which aids alignment and minimises mechanical play. The stem is hollow, with a nut embedded at its open end, enabling it to be driven by a threaded lead screw under the control of an electrical actuator. The piston head of the plunger incorporates an O-ring to provide a leak-proof seal between piston and the cylindrical chamber (Figure 2). Different screw-in orifice diameters can be easily swapped in and out. By way of example, our prototype includes a set of four interchangeable orifices with diameters that range from 10 mm to 25 mm in steps of 5 mm (Figure 3). These generate rings of several centimetres diameter with characteristics that are relevant to human physiology.

2.3 Programmable Actuator

The nut/lead screw arrangement of the piston enables it to be driven by a linear stepper motor - this constitutes the actuator of the ring vortex generator. The plunger nut moves along the rotating screw to generate plunger motion. A Nema 23 external linear stepper motor drives the threaded screw of length 150 mm (Nema 23 external linear actuator, OMC Corporation Limited, Nanjing, China). The motor is fixed with respect to the imaging tank through a rigid mounting bracket. Power is delivered through a digital stepper driver (OMC Corporation Limited, Nanjing, China) which has connections to a switching 150 W power supply (OMC Corporation Limited, Nanjing, China). Motor control is delivered via an Arduino Uno (Atmega328) microcontroller (Atmel Corporation, San

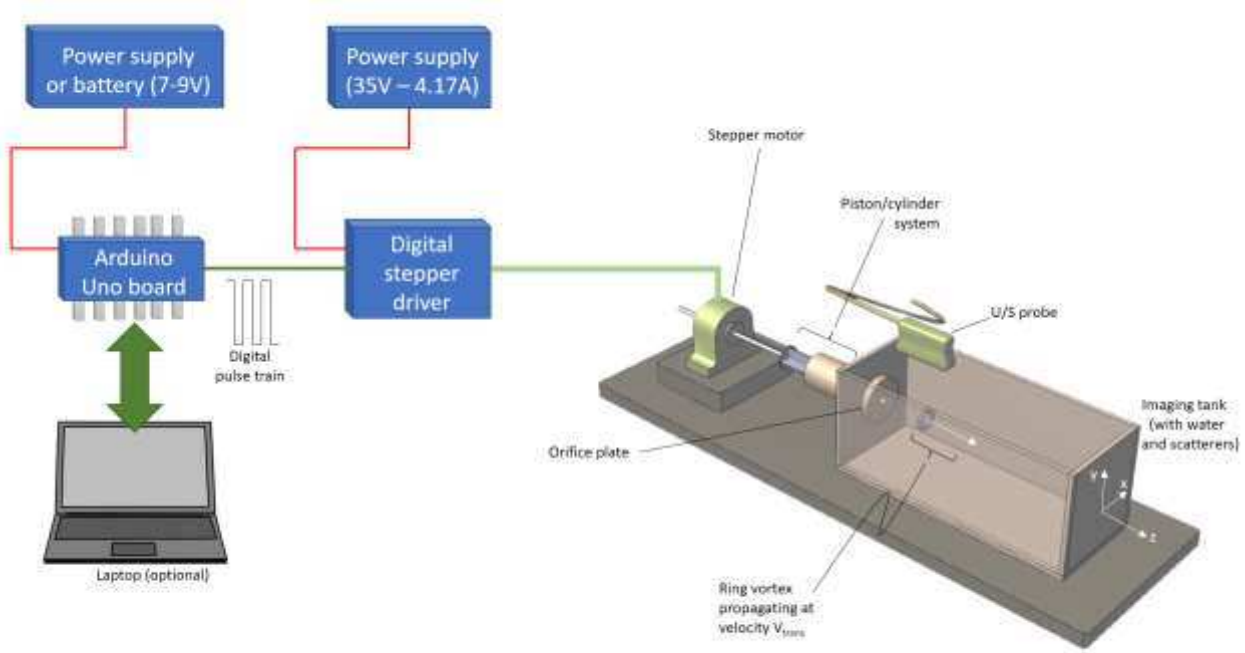

Figure 4a. *Block-diagram of the ring vortex flow phantom, illustrating vortex propagation at velocity* V_{trans}

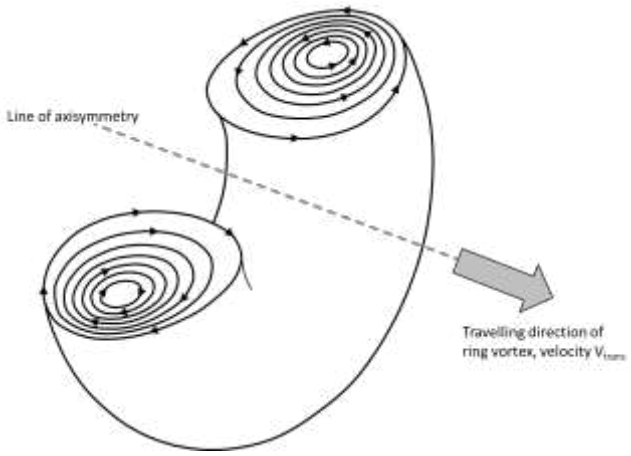

Figure 4b. *Layers of concentric circulating flow constituting the toroidal core, propel the ring vortex forward along its axis of symmetry at velocity V_{trans}*

Jose, California, USA). The minimum linear step displacement provided by the system (driver-motor-nut-lead screw) is 0.02 mm with an accuracy of +/-5%, as declared by the manufacturer. The current supplied to the motor is limited to 2.69 A (RMS current) in order to avoid overheating. The Atmega328 enables programmable displacement of the actuator, supporting custom variable displacement/velocity profiles. The pins of the microcontroller are connected to a power supply circuit (or to a Laptop) and to the stepper driver. The digital system relies on CMOS logic (0-5V), with a square-wave signal of varying frequency (from 0.5 kHz to 1 kHz) but fixed duty cycle (50%) controlling the digital motor displacement. A schematic block diagram of the system is shown in Figure 4. The total cost of all the electronic components is less than one hundred Euros at the time of writing (2019).

2.4 The Assembled System

The interconnection of these components provides the system depicted in Figure 5. The actuator is programmed to deliver a preconfigured displacement profile (eg. top-hat) that moves the piston through the cylinder and propels a slug of fluid through the orifice (e.g. 3 cm^3 of displaced fluid in 50 ms). This results in a controlled, propagating ring vortex of an orifice-dependent size that travels steadily (with velocities < 1 ms^{-1}) along the length of the tank (Figure 4). Images captured by an imaging system can be referenced to the features of the flow, permitting characterisation of imaging system performance. Bulk features (ring speed, size) are readily established through simple optical/video methods [20] whereas finer details of the flow benefit from technologies such as particle image velocimetry (PIV) or even computational fluid dynamics (CFD) [21].

3. Demonstration and Application

A summary of the experimental configurations used to demonstrate the vortex flows is listed in Table 1. Reynolds number calculations are based on flow through the orifice generating the ring ($Re = \rho Vd/\mu$; ρ-density, V-velocity, d-diameter, μ-viscosity). In order to confirm the functionality of the phantom design,

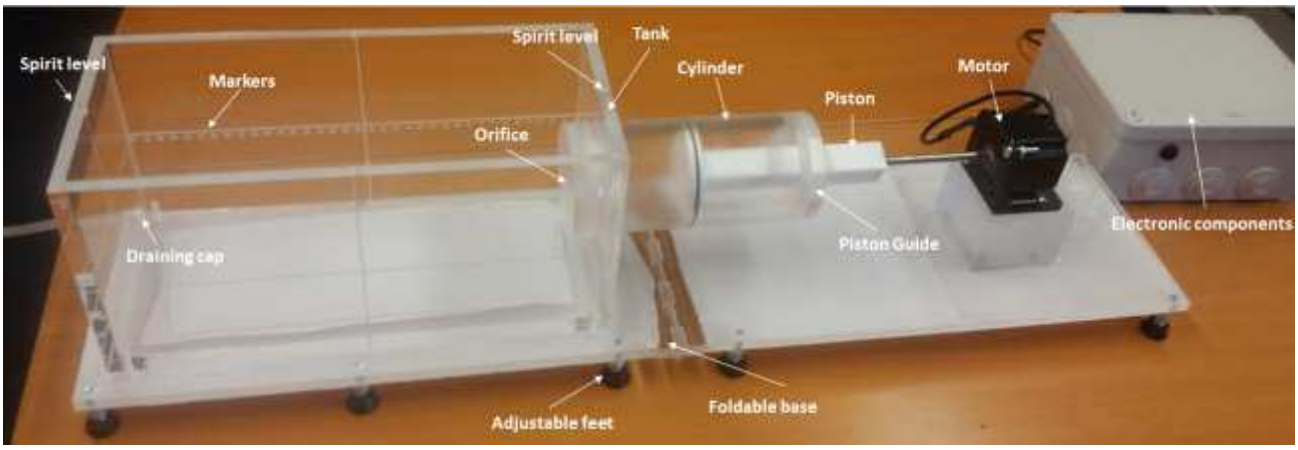

Figure 5. *Assembled ring vortex flow phantom.*

Configuration	*Orifice Diam. (mm)*	*Piston Speed (cm/s)*	*Piston Displacement (mm)*	*Re*
1	10	2	0.8	9800
2	10	1.33	0.8	6517
3	15	2	0.8	6534
4	15	2	0.6	6534
5	15	1.33	0.8	4345
6	15	1	0.8	3267
7	20	2	0.8	4900
8	20	1.33	0.8	3258
9	25	2	0.8	3920
10	25	1.33	0.8	2606

Table 1. *Summary of the flow generating conditions, with Reynolds number at the throat of the orifice cited. Each configuration was repeated ten times to evaluate reproducibility*

two different measurement methods were used to characterise the generated flows, namely optical/video measurements and Laser-PIV; details are provided in sections 3.1 and 3.2 below. Optical/video measurements were accomplished on the premises of Leeds Test Objects Ltd (Leeds Test Objects Ltd, Boroughbridge, United Kingdom) as previously described by Ferrari et al [20]. A complementary method - Laser-PIV – was also employed, which is a well-established technique for quantitative measurement of complex flow velocity fields [22,23]. The PIV work was undertaken at the Cardiovascular Science department of the University of Sheffield (Royal Hallamshire Hospital, Sheffield, United Kingdom) and performed with a calibrated LaVision system (LaVision GmbH, Gottingen, Germany). The PIV methodology followed that described by Wieneke [24], with calibration procedures performed under the supervision of a LaVisionUK Ltd (LaVisionUK Ltd, Bicester, United Kingdom) application consultant. For both modalities (Optical/video and Laser-PIV) the imaging tank (with relevant orifice) and piston channel were filled with water. Data was collected from two identically constructed phantoms, both of which were produced by Leeds Test Objects Ltd (Leeds Test Objects Ltd, Boroughbridge, United Kingdom). Experiments were conducted for all four orifice sizes provided with the phantom. A single programmed piston displacement of 0.8+/-0.04 mm, and two principal piston speeds, 2+/-0.1 cm/s and 1.33+/-0.06 cm/s, were used for this evaluation. The piston speed of 2 cm/s was of interest because it drives the motor close to its maximum achievable speed. Ten separate ring vortices were generated, enabling the reproducibility of rings produced by the phantom to be quantified. Finally, a further piston displacement of 0.6+/-0.03 mm and piston speed 1 cm/s was also tested.

3.1 Optical/video acquisition

The optical/video system required a few drops of food colouring to be mixed with the volume of water in the piston cylinder, to enable a visible coloured ring vortex to be produced. Vortex progress was captured at 25 frames per second using a Sony camera HDR-PJ220E (Sony Corporation, Tokyo, Japan). The camera was placed on a tripod at a distance of 3.8 m from the phantom, obtaining a clear view through the sides of the transparent tank. A telephoto lens at 32x extended zoom ensured that the images contained minimal perspective error. The field of view was centred on a volume of interest within the tank, 9 cm from the orifice, capturing details of ring vortex behaviour over a 10 cm region. This zone was chosen as the region of interest for all measurements (including PIV). In addition, a 1/100sec universal counter-timer (RS Components Ltd, Stock No 612-445) was placed within the field of view of the images to provide visible timing data in support of the measurements. Distance measurements from still frames enabled characterisation of vortex ring position and translational speed. Vortex ring velocities (V_{trans}) were calculated by measuring the translational displacement of the vortex ring along the long axis of the tank (Figure 4) in consecutive frames, combined with the timing data from the video images. Average translational velocity as a function of vortex ring position in the tank (with reference to the position markers visible in Figure 1) was calculated from the acquisition of 10 vortex rings for each of the

configurations listed in Table 1. Error bars indicate ± 1 SD (Figs. 6, 7).

3.2 Laser-PIV acquisition

The Laser-PIV setup required neutrally buoyant scattering particles mixed throughout the tank/cylinder system to provide satisfactory conditions for flow capture using the stereo Laser-PIV technique. Fluorescent particles of size 10-20 micron were mixed within the volume of water, which was illuminated by a laser sheet that cut the propagating ring through its centre in the vertical plane. Reconstruction of particle displacement using two camera projections (stereoscopic view) and digital image correlation allowed the reconstruction of the flow field [24] at a spatial resolution of 0.4 mm and temporal steps of 0.071 s (14 Hz). Accuracy of the instantaneous velocities of the PIV system is declared by LaVisionUK Ltd (LaVisionUK Ltd, Bicester, United Kingdom) to be better than +/-0.1%. Mapping the flow field of the V_z components (ie. along the z-axis of Figure 4) at each frame and knowing the frame rate of the acquisition (14 fps), the translational velocity of the ring was calculated. Average vortex ring translational velocities (V_{trans}, Figure 4) and standard deviation values, as a function of the vortex ring position in the tank (with reference to position markers in Figure 1), were obtained from the multiple vortex ring acquisitions listed in Table 1.

4. Results

4.1 Optical/Video measurements

Average vortex ring translational velocities (V_{trans} with standard deviation expressed by the error bars) as a function of vortex ring position are plotted in figs 6,7

Translational velocity (cm/s) vs phantom position - laser PIV (dash lines) and optical dye data (solid lines)
Different orifices and settings – configuration 1 to 5, table 1

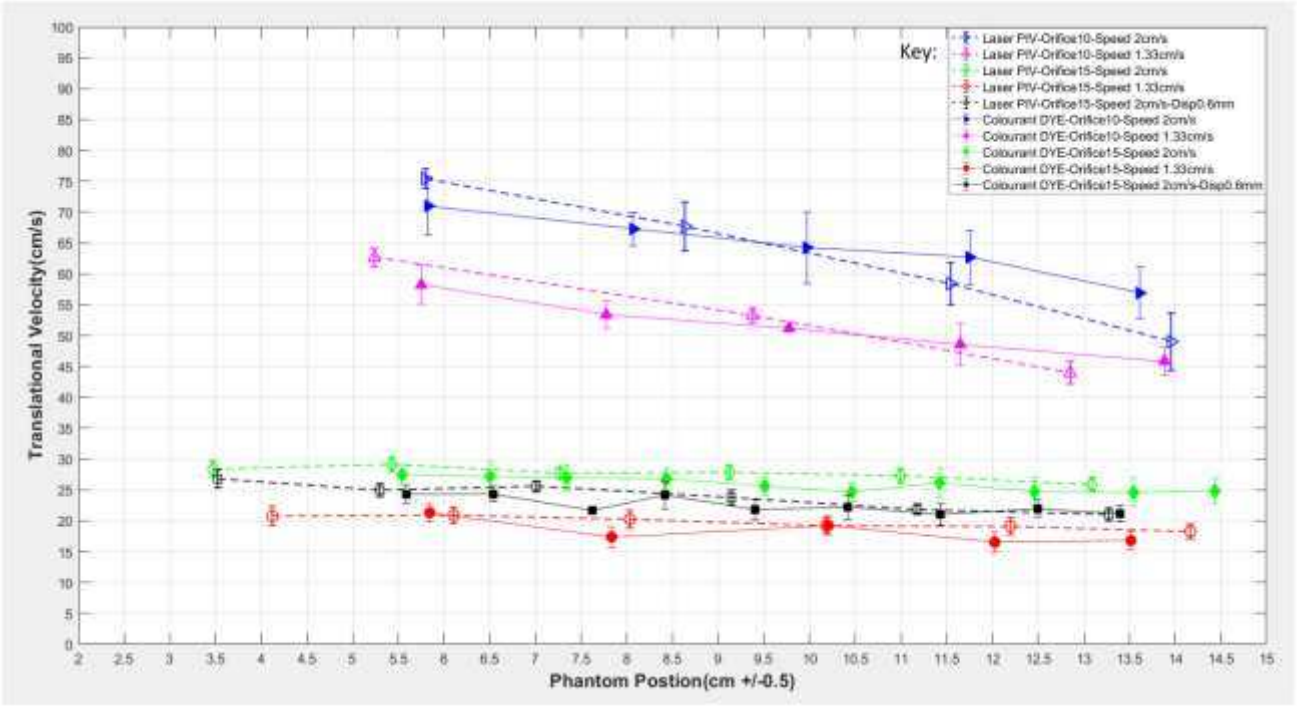

Figure 6. *Laser-PIV and coloured dye translational velocity measurements relevant to configuration 1 to 5 (Table 1). Each configuration corresponds to a particular marker/shape combination enabling direct comparison of optical/PIV measurements. Laser-PIV data are plotted with dashed lines while coloured dye data uses solid markers with bold lines. Error bars represent the standard deviation values on 10 acquisitions.*

Translational velocity (cm/s) vs phantom position - laser PIV (dash lines) and optical dye data (solid lines)
Different orifices and settings – configuration 5 to 10, table 1

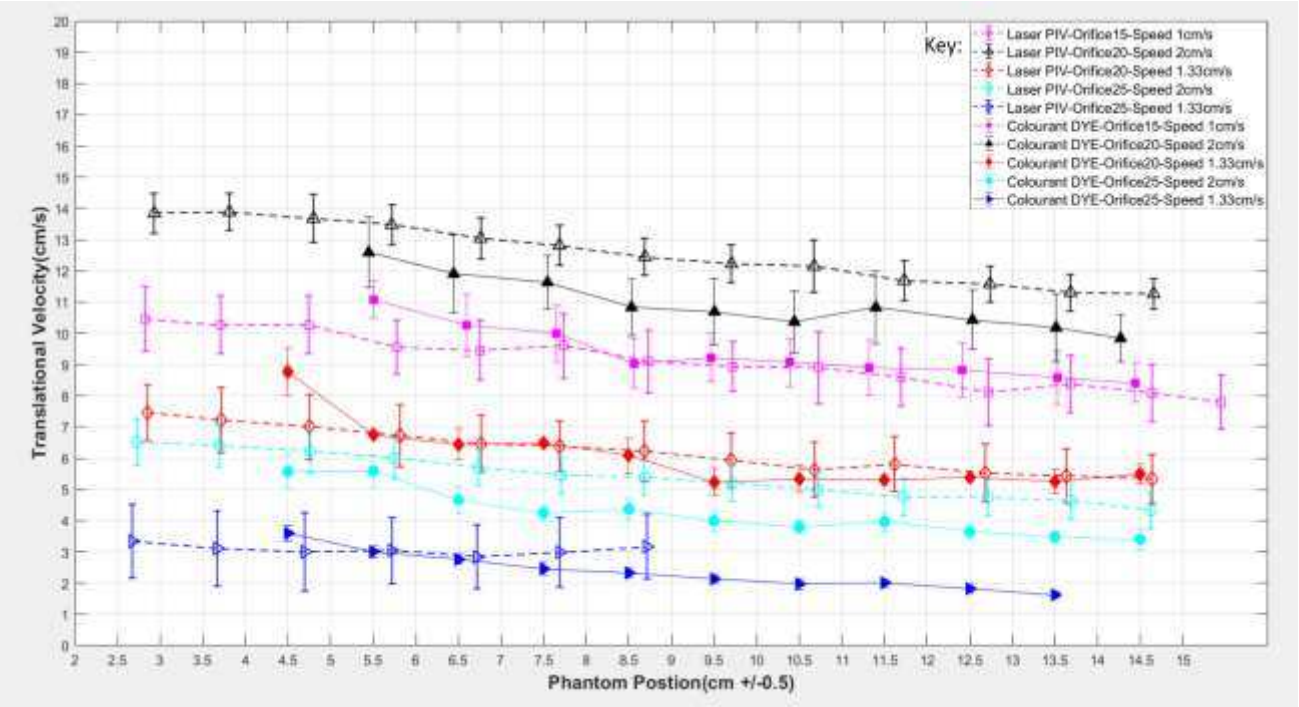

Figure 7. *Laser-PIV and coloured dye translational velocity measurements relevant to configuration 6 to 10 (Table 1). Each configuration corresponds to a particular marker/shape combination enabling direct comparison of optical/PIV measurements. Laser-PIV data are plotted with dashed lines while coloured dye data uses solid markers with bold lines. Error bars represent the standard deviation values on 10 acquisitions.*

(see Table 1 for the configurations tested). Position is referenced to the tank markers visible in Figures 1 and 5. For improved clarity, results for the configurations that produced faster ring vortices (from 15 cm/s to 80 cm/s) are shown in Figure 6 while results from slower configurations (from 0 cm/s to 15 cm/s) are shown in Figure 7. In order to compare the optical data directly with the Laser-PIV translational velocity measurements, each selected configuration (Table 1) corresponds to a specific colour and marker-shape combination. Optical/video results are expressed as bold lines with filled markers, whereas the PIV data is presented as open markers and dashed lines. In each case, variability within 10 runs is presented as +/-1SD on the plots and cited as coefficient of variation (%) within the text. Such errors calculated with the optical/video method are always less than +/-10%.

4.2 Laser-PIV

For consistency, average PIV vortex ring translational velocities (V_{trans}, Figure 4) with standard deviation are also plotted (dashed lines) as a function of vortex ring position (tank reference position markers in Figure 1). These are calculated from 10 vortex ring acquisitions for each of the settings listed in Table 1 (as for the optical/video method). Piston configurations providing faster ring vortices (from 15 cm/s to 80 cm/s) are shown in Figure 6 while results for slower configurations (from 0 cm/s to 15 cm/s) are shown in Figure 7. Relative errors were calculated as for the optical/video experiment, and the varying configurations confirm very similar behaviour to the optical results. Notably, the error increases for slower vortex ring configurations (e.g. Configuration 10, Table 1). On the other hand, an orifice of 10 mm, with

Vortex ring position (cm) vs Time (s) – five different configurations (see table 1)

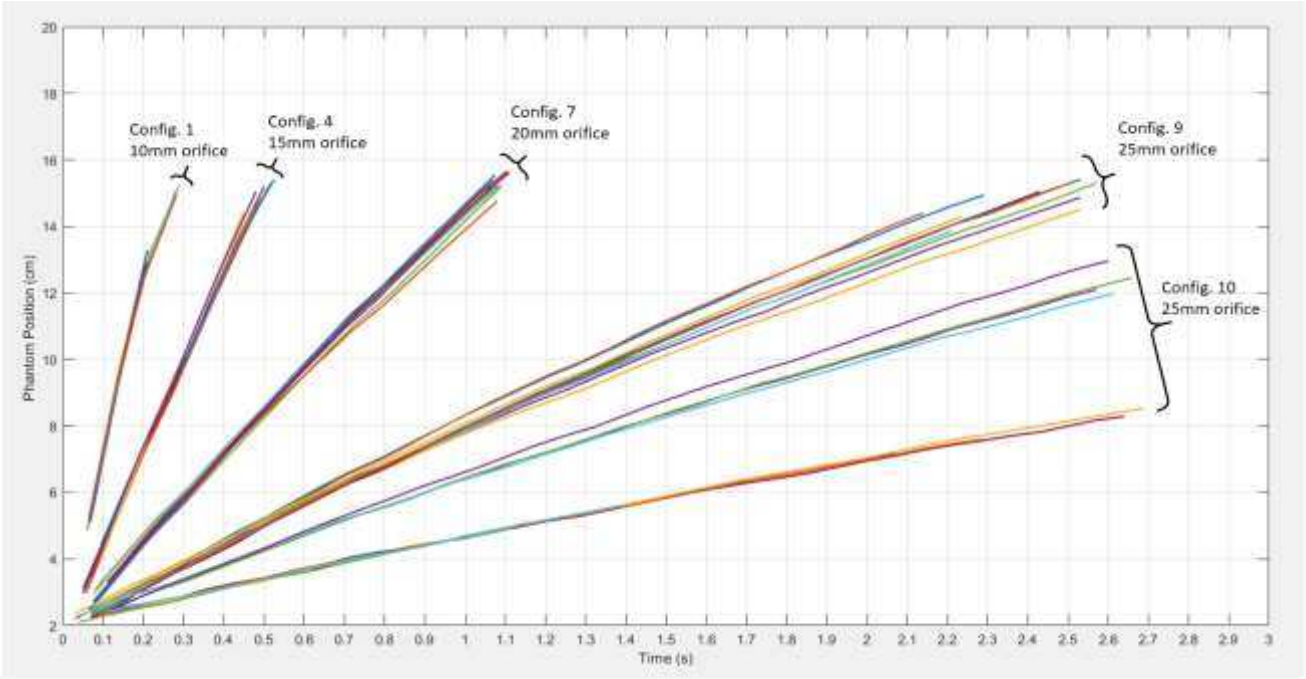

Figure 8: *This plot present data for configurations 1, 4, 7, 9, 10 (table 1). The dispersion in ring speed is apparent from this representative collection of experimental runs illustrating ring position vs time. Ring velocity can be determined from line gradient, and variability <10% for each group (except for the 25mm orifice example). Notably, the rings of lower energy and speed are more variable. With a 2.5cm diameter orifice, and lower pump speeds, the ring might not even form.*

piston speed 1.33 cm/s and piston displacement of 0.8 mm, provided the lowest percentage variability (error < +/-3%). For completeness, ring position as a function of time for a selection of rings is plotted in figure 8.

5. Discussion

In this paper, bulk flow performance has been assessed using two identical systems, undertaken at two different places (Leeds and Sheffield), two weeks apart. Results provided by two different measurement methods - Laser-PIV and optical/video measurements – have enabled performance of ring vortex production to be compared, and the consistency of the results across these scenarios is a measure of the stability and predictability of the flow phantom. Translational velocity averages and error values from the acquisition of 10 vortex rings for a given configuration (Fig 6,7) demonstrate variability of less than +/- 10%, with worst performance occurring for the slower configurations. The Laser-PIV technique confirms that there are velocities where the vortex ring has high stability, with error less than +/- 3% for the best case, (Configuration 2, Table 1). Interestingly, vortices generated with high velocities (60-80 cm/s, Configuration 1 and Configuration 2, Table 1) are clearly more dissipative in their early stages (showing an initial velocity decay) whilst vortices with velocities lower than 30 cm/s travel steadily, with little change in velocity or ring size across the whole length of the phantom tank. It is worth noting that our analysis has focussed on bulk flow characteristics (eg. translational vortex ring speed V_{trans}) but for completeness, further work is needed to assess the micro-flow environment in addition to the macro-flow characteristics described here. The PIV offers some insights (Fig 9a). Micro-flow characterisation is crucial for encouraging the use of the ring vortex as a complex flow benchmark for advanced flow velocity estimation

imaging techniques (eg. Vector Flow Imaging). For proof of concept purposes, its application in the context of a clinical Doppler imaging system is illustrated in the images of figure 9. With the flow seeded with cornflour, the B-scan (Fig 9b) captures the cross-sectional toroidal structure of the propagating ring, whereas the colour Doppler image (Fig 9c) obtained in the same plane exposes flow direction as the ring vortex travels across the field of view. Qualitatively, the Doppler demonstrates an appropriate quadrantal colour signature in accordance with the circulating toroidal flow detected by the PIV (compare with figure 9a), although fig 9c also evidences a trail of persistence artefacts too. State of the art vector flow imaging systems have also been demonstrating use of this technology as described by Badescu et al [38]. The encouraging reproducibility of the flow phantom means that flow measurement exercises can be reliably repeated, enabling deeper examination of imaging system performance.

In respect of ring vortex performance, Gharib observed that vortex ring generation depends on a non-dimensional parameter, described [25] as formation time or formation number. For a given geometry, the formation number is described as $T^* = (\bar{U}/D)T_p$, where $\bar{U}$ is the mean velocity of the piston, D is the orifice diameter and T_p is the duration of the piston impulse. There is also a critical value for the formation number, below which the ring will not form [25]. Although the actuator offers pre-programmed modes, the computer code is open-source, so the device has great flexibility and allows the user to vary experimentally each element of Gharib's formula. Consequently, a range of vortex rings can be created. Different orifice sizes (D) can also be easily interchanged, providing different vortex diameters. By simply altering the stepper motor speed ($\bar{U}$), the piston displacement extent (T_p) or the orifice size (D), vortex rings with different Reynolds Numbers, different volumes, core thicknesses, diameters and different velocities can be generated. A detailed review of the evolution and stability of vortex rings in viscous fluids and the dependency on the initial conditions (formation time and Reynolds number) is provided by Tinaikar et al [26].

(a) (b) (c)

Figure 9: Image *(a) displays a colormap derived from the PIV data, depicting the y-component (vertical direction) of the fluid velocities within the ring vortex. (b) shows the structure of the ring (vertical cross-section) captured by the B-scan mode of a Doppler scanner. The color Doppler image (c) clarifies flow toward/away from the probe (placed at the top of the image) and apart from the persistence artefact, appropriately resembles the PIV data of image (a).*

The ring vortex flow is well suited to its role as a reference flow because it offers characteristics like stability, predictability, reproducibility and controllability [20,21,26,27]. Ring vortices are flow patterns that are relevant to both healthy and pathophysiological *in vivo* conditions

[1,2,8,28,29,30,31,32,33,34,35,36]. Vortex rings are natural fluid phenomena that are known to balance flow within the chambers of the heart or may be observed in the presence of vessel bifurcations or pathological conditions, such as stenosis and aneurysm. Detection and quantitative characterisation of these complex flow patterns can provide a considerable amount of information about the correct functioning of valves [30], vessels [28] and myocardium [1]. However, the relevance of the flow generated by the phantom goes beyond physiology. At a more fundamental level, any complex flow can be considered to be composed of simpler flow elements, such as velocity gradients, acceleration/pulsatility and vorticity. The flexibility of the ring vortex design allows such elements to be delivered under controlled conditions. For the purposes of QA, the flow must also be repeatable, producing predictable flows that are insensitive to subtleties of the generating conditions or environment. Importantly, the measurement processes described in this paper indicate that realistic tolerances for these reproducible flows can be asserted – hence the utility of this design as a complex flow phantom.

Placing this work in a broader context, analysis of the market and literature indicates that despite the availability of numerous flow test objects, they can be expensive, difficult to manufacture and may suffer from significant limitations [15,16]. Furthermore, their accuracy and supporting quality assurance metrics are often not clarified by the manufacturers [16,18]. Currently, there is a real paucity of phantoms for Quality Control of the new generation of medical Ultrasound scanners that support Vector Flow Imaging and there are no technologies on the market that provide stable complex flow structures against which the new research-capable velocity-estimation-Doppler-algorithms can be validated. Consequently, the quality control and calibration of flow medical imaging scanners continues to be challenging. This is especially relevant to new technologies where well specified quality control protocols are desirable [16]. A flow phantom should provide a spectrum of blood velocities typical of the *in vivo* situation [19], allowing waveform analysis, volume flow and speed flow quantification for the calibration of the medical equipment [18,19,37]. Arguably, the ideal flow phantom would be multimodal, offering reproducible flows (at least to within known and well specified tolerances), with a range of features, velocities, volumes and Reynolds numbers.

With a longer-term ambition to compare flow imaging performance between different flow medical imaging modalities (Ultrasound, MRI and CT) - both for clinical and research purposes - the ring vortex phantom has been entirely manufactured from PMMA (except for the motor). PMMA has been chosen because it is durable, waterproof, can be easily manufactured in clear form or with different colours and its attenuation of X-Rays is comparable with human soft tissues at diagnostic energies [39]. However, since the motor is ferromagnetic, a design adaptation is necessary for MRI compatibility. For instance, the motor could be replaced with an ultrasonic unit [40] or with an MRI compatible linear motion system (e.g. http://www.simutec.com/Products/motionstages.html). MRI compatible motion systems are much more expensive and this would significantly increase the cost of the phantom. A Magnetic Resonance compatible ring vortex flow has already been demonstrated by Toger et al [27,36], and although the phantom proposed in this paper exploits a comparable technology, our design aspires to be low-cost, compact, portable, easy to manufacture, programmable. Future work will extend the assessment presented here to include comparative studies between medical imaging modalities (Ultrasound, CT, and with some adaptation MRI) and optical modalities (Laser-PIV, Laser-diode) to further assess reliability, long-term stability and detailed flow performance. Currently, four identical phantom systems have been manufactured and are currently being evaluated in the United Kingdom and France within both research and clinical environments, in order to identify potential improvements to the design. In an environment where the quality control of flow medical imaging scanners is still challenging and

confusing, this technology offers support for both research and clinical imaging activities.

6. Conclusion

A technical specification for the design of a novel, cost-effective, portable complex flow test object currently compatible with ultrasound modalities has been provided. Early experience indicates that the technology has the characteristics suited to basic and more advanced ultrasound quality control checks at research and clinical level. The design could be adapted for comparative studies with different medical imaging modalities, such as Ultrasound and X-Rays. Significant adaptation is required if Magnetic Resonance compatibility is to be considered. The phantom as described, demonstrates that it can be reproducibly manufactured to deliver consistent performance within specified tolerances.

Disclosure Statement

The authors report no conflict of interest.

Funding

This work is funded by the European Commission through the H2020 Marie Sklodowska-Curie European VPH-CaSE Training Network (www.vph-case.eu), GA No. 642612.

The vortex ring-based flow phantom has been manufactured using the facilities of Leeds Test Objects Ltd (Leeds Test Objects Ltd, Boroughbridge, UK), as beneficiary and partner of the VPH-CaSE consortium (http://www.vph-case.eu/, EU Horizon 2020 funding Marie Curie Training Network).

References

1. Pedrizzetti G, La Canna G, Alfieri O et al. The vortex—an early predictor of cardiovascular outcome?. Nat Rev Cardiol. 2014;11(9):545-553.
2. Arvidsson PM, Kovács SJ, Töger J, et al. Vortex ring behaviour provides the epigenetic blueprint for the human heart. Sci Rep. 2016;6:22021.
3. Ricotta JJ, Pagan J, Xenos M, Alemu Y et al. Cardiovascular disease management: the need for better diagnostics. Med Biol Eng Comput. 2008; 46(11):1059-1068.
4. Garcia J, Barker AJ and Markl M. The Role of Imaging of Flow Patterns by 4D Flow MRI in Aortic Stenosis. JAAC: Cardiovascular Imaging. 2019;12(2):252-266.
5. Sengupta PP, Pedrizzetti G, Kilner PJ et al. Emerging trends in CV flow visualization. JACC Cardiovasc Imaging. 2012;5(3):305-316.
6. Jensen JA, Nikolov SI, Yu ACH et al. Ultrasound Vector Flow Imaging-Part I: Sequential Systems. IEEE Trans Ultrason Ferroelectr Freq Control. 2016;63(11):1704-1721.
7. Hansen KL, Møller-Sørensen H, Kjaergaard J et al. Vector Flow Imaging Compared with Conventional Doppler Ultrasound and Thermodilution for Estimation of Blood Flow in the Ascending Aorta. Ultrason Imaging. 2017;39(1):3-18.
8. Hoskins PR. Haemodynamics and blood flow measured using ultrasound imaging. Proc Inst Mech Eng Part H J Eng Med. 2010;224(2):255-271.
9. Garcia D, Del Alamo JC, Tanne D et al. Two-dimensional intraventricular flow mapping by digital processing conventional color-doppler echocardiography images. IEEE Trans Med Imaging. 2010;29(10):1701-1713.
10. Westerdale J, Belohlavek M, McMahon EM et al. Flow Velocity Vector Fields by Ultrasound Particle Imaging Velocimetry. J Ultrasound Med. 2011;30(2):187-195.
11. Kokkalis E, Cookson AN and Stonebridge PA. Comparison of Vortical Structures Induced by Arteriovenous Grafts Using Vector Doppler Ultrasound. Ultrasound Med Biol. 2015;41(3):760-74.
12. Badescu E, Petrusca L, Garcia D et al. Towards 3-D tissue doppler ultrafast echocardiography: An in vitro study. Paper presented at: IEEE International Ultrasonics Symposium, IUS; 2017 September 6-9; Washington, DC.
13. Badescu E, Bujoreanu D, Petrusca L, Friboulet D and Liebgott H 2017-b Multi-line transmission for 3D ultrasound imaging: An experimental study. Paper presented at: IEEE International Ultrasonics Symposium, IUS; 2017 September 6-9; Washington, DC.
14. Jensen J A, Pihl MJ, Olesen JB et al. New Developments in Vector Velocity Imaging using

the Transverse Oscillation Approach. In Proceedings of SPIE: Medical Imaging 2013: Ultrasonic Imaging, Tomography, and Therapy. 2013;8675**:**86750F.
15. Institute of Physics and Engineering in Medicine. Report 102 - Quality Assurance of Ultrasound Imaging Systems. Manchester: Stephen Russell; 2010.
16. Browne JE. A Review of Doppler Ultrasound Quality Assurance Protocols and Test Devices. Phys Medica. 2014;30(7):742-751.
17. Cournane S, Fagan AJ and Browne JE. An audit of a hospital-based Doppler ultrasound quality control protocol using a commercial string Doppler phantom. Phys Medica. 2014; 30(3):380-384.
18. Dudley N and McKenna M. Options for assuring Doppler velocity accuracy. Paper presented at: IPEM - The Physics & Technology of Medical Ultrasound. 2017 April 4; York, United Kingdom.
19. British Standard Institution (BSI). Ultrasonics. Flow measurement systems. Flow test object. BSI; 2002. Standard No. BS EN 61685:2002, IEC 61685:2001.
20. Ferrari S, Ambrogio S, Walker A et al. The ring vortex: A candidate for a liquid-based complex flow phantom for medical imaging. Lect Notes Comput Vis Biomech. 2018;27:893-902
21. Ferrari S, Ambrogio S, Walker A et al. The Ring Vortex: Concepts for a Novel Complex Flow Phantom for Medical Imaging Open J Med Imaging. 2017; 7(1):28-41.
22. Grant I. Particle image velocimetry: a review. Proc Inst Mech Eng Part C J Mech Eng Sci. 1997;211(1):55-76.
23. Westerweel J, Elsinga GE and Adrian RJ. Particle Image Velocimetry for Complex and Turbulent Flows. Annual Review of Fluid Mechanics. 2013;45(1):409–436.
24. Wieneke B. Stereo-PIV using self-calibration on particle images Experiments in Fluids. 2005;39: 267-280.
25. Gharib M, Rambod E and Shariff K. A universal time scale for vortex ring formation. J Fluid Mech. 1998;360:121-140.
26. Tinaikar A, Advaith S and Basu S. Understanding evolution of vortex rings in viscous fluids. J Fluid Mech. 2018;836:873-909.
27. Töger J, Bidhult S, Revstedt J et al. Independent validation of four-dimensional flow MR velocities and vortex ring volume using particle imaging velocimetry and planar laser-Induced fluorescence. Magn Reson Med. 2016;75(3):1064-1075.
28. Hoskins PR. Peak velocity estimation in arterial stenosis models using colour vector Doppler. Ultrasound Med Biol. 1997;23(6):889-897.
29. Kheradvar A and Gharib M. Influence of Ventricular Pressure Drop on Mitral Annulus Dynamics Through the Process of Vortex Ring Formation. Annals of Biomedical Engineering. 2007:37(1):1-13.
30. Kheradvar A and Gharib M. On Mitral Valve Dynamics and its Connection to Early Diastolic Flow. Annals of Biomedical Engineering. 2009;35(12):2050-2064.
31. Querzoli G, Fortini S and Cenedese A. Effect of the prosthetic mitral valve on vortex dynamics and turbulence of the left ventricular flow. Phys Fluids. 2010;22(4):1-10.
32. Kheradvar A, Assadi R, Falahatpisheh A et al. Assessment of transmitral vortex formation in patients with diastolic dysfunction. J Am Soc Echocardiogr. 2012;25(2):220-227.
33. Töger J, Carlsson M, Soderlind G et al. Volume tracking: a new method for quantitative assessment and visualization of intracardiac blood flow from three-dimensional, time-resolved, three-component magnetic resonance velocity mapping. BMC Med Imaging. 2011;11:10.
34. Domenichini F and Pedrizzetti G. Intraventricular vortex flow changes in the infarcted left ventricle: Numerical results in an idealised 3D shape. Computer methods in biomechanics and biomedical engineering. 2011;14:95-101.
35. Kheradvar A and Pedrizzetti G. Vortex Formation in the Cardiovascular System. London: Springer-Verlag; 2012.
36. Töger J, Kanski M, Arvidsson PM et al. Vortex-ring mixing as a measure of diastolic function of the human heart: Phantom validation and initial observations in healthy volunteers and patients with heart failure. J Magn Reson Imaging. 2016;43(6):1386-1397.

37. Hoskins PR, Anderson T and McDicken WN. A computer controlled flow phantom for generation of physiological Doppler waveforms. Phys Med Biol. 1989;34(11):1709-1717.
38. Badescu E, Ambrogio S, Fenner J et al. Vortex Ring Phantom for Investigation of Ultrasound Vector Flow Imaging. Paper presented at: IEEE International Ultrasonics Symposium, IUS; 2018 October 22-25; Kobe, Japan.
39. The International Commission on Radiation Units and Measurements. Report 87-Radiation Dose and Image-Quality Assessment in Computed Tomography. Journal of the ICRU. 2012;12(1):1-149.
40. Tavallaei MA, Johnson PM, Liu J et al. Design and evaluation of an MRI-compatible linear motion stage. Med Phys. 2016;43(1):62-71.